EVALUATION OF THE OVERFLOW FAILURE SCENARIO AND HYDROGRAPH OF AN EMBANKMENT DAM WITH A CONCRETE UPSTREAM SLOPE PROTECTION

François Chiganne, Claude Marche et Tew-Fik Mahdi

Département des génies civil, géologique et des mines

École Polytechnique de Montréal

C.P. 6079, Succ. Centreville,

Montréal, Québec, Canada, H3C 3A7.

* Auteur correspondant: tewfik.mahdi@polymtl.ca, Tel: (514) 340-4711 ext. 5874.

Abstract : The standard procedure in Quebec, Canada, for evaluating the failure of an embankment dam, per the *Loi sur la sécurité des barrages,* specifies a 30 minute long failure scenario with a breach width equal to four times the maximal height of the dam. We demonstrate a new method for evaluating the flood overtopping failure scenario for embankment dams with concrete upstream slope protection, using Toulnustouc Dam for example computations. Our new methodology computes safety factors for a range of potential failure mechanisms taking into account geotechnical, hydraulic, and structural factors. We compile the results of our investigations of the various dam failure mechanisms and compare the corresponding dam failure hydrographs to the current hydrograph specified in the standard analysis procedures. Our investigations tend to invalidate the current standard procedures for evaluating the failure of rockfill dams with concrete upstream faces, by indicating that the current standard procedures underestimate the peak failure discharge and overestimate the time to the peak discharge.

Key words: dam failure, overtopping, rockfill dam, failure hydrograh.

1. Introduction

The oldest known dam is an earth-fill dam constructed in the Garawi Valley in Egypt about 3000 years ago. Although our knowledge of dam construction techniques and reservoir operations has increased dramatically over the years, the potential for dam failures still poses a significant threat to communities around the world. Dam failures have been responsible for more than 8000 deaths and hundreds of millions of dollars in economic losses since 1900 (Marche, 2008).

These failures were primary due to inadequate construction materials and/or design of the dam structure and the corresponding spillway structure. In order to increase dam safety, standard procedures, regulations and models have been established to diminish the risk of failure due to overtopping (i.e., establishment of minimal discharge capacity etc.), and to better define the downstream flood hazard zone corresponding to a catastrophic dam failure.

These standard procedures and regulations are not intended to represent specific failure scenarios, they are based on information from former failures. For embankment dams and overtopping failures, the standard procedures, in Quebec, Canada, specify the formation, in 30 minutes, of a breach with a bottom width equal to four times the maximum height of the dam (Marche, 2008). Given these specifications for the breach geometry, it is possible to calculate a failure hydrograph and to delimit the corresponding flood hazard areas.

Masson (2009) compares the failure hydrographs of an embankment dam (dyke Moncouche) with a concrete curtain calculated using the standard procedures specified in the current regulations with the results of a methodology based on the calculation of structural safety factors, whose validities were confirmed by an experimental model. The scale effect was taken into account in this work by adjusting erosion depths, overtopping levels, breach discharges and the time scale, which strengthened the validity of the results. First, these results highlighted that the duration of the dam failure, 30 minutes, may be overestimated (of about 15%). Then, it was demonstrated that the current regulation doesn't take into account dams' specificities such as a rising of the dam or the installation of a parapet, these measures security being able to increase the safety of the dam by increasing failure's duration and decreasing the peak discharge. Finally, the hypothesis that the discharge increases linearly

is questioned. Structural elements, such as a concrete curtain, can indeed lead to several brutal increases of the discharge. Our goal in this article is to highlight the differences between overtopping scenarios for an embankment dam with a concrete upstream face corresponding to the current standard procedures with those calculated based on different failure mechanisms not considered in the current regulations.

Since we use the Toulnustouc Dam to demonstrate our methodology, we first describe the key characteristics of this dam. Next we describe our metholodologies for calculating a series of safety factors corresponding to the following failure mechanisms: a) the landslide safety factor is calculated based on the "Multiple Wedge Analysis" (U.S. Army Corps of Engineers, 1995); b) the safety factor for dam failure caused by the motion of the crest material is evaluated using a seepage model for the dam and a study of the forces acting on a rock on the downstream side of the crest; c) dam failure caused by the motion of the downstream bottom of the dam is linked to the velocity and the hydraulic gradient of flow through the dam using the studies by Wilkins (1956); and d) failure of the parapet and the upstream slope protection are evaluated using strength of material analyses.
To demonstrate our methodologies for calculating a series of safety factors corresponding to different failure mechanisms, we provide example calculations corresponding to a specific flood scenario for Toulnustouc Dam. We compare the results of these analyses, including the corresponding dam failure hydrograph, with those using the standard procedures specified in current regulations.

2. Toulnustouc dam

The Toulnustouc dam is located in the Côte-Nord area, in Rivière-aux-Outardes. It’s an embankment dam with an upstream concrete mask, 77 m high and 535 m long. The reservoir reaches a maximum depth of 72.3 m on the upstream side of the dam. The dam is built with large stones (figure 1 and 2), types 8C, 8B, 8A and 7D. The 8A and 7B layers (also called “mask”) are only used to stabilize the foundation of the upstream slope protection of

the dam. Most of the rocks have a diameter of about 1 m. Figures 1 and 2 illustrate the overall geometry of the dam and give details of the crest geometry.

The concrete upstream slope protection is 300 mm thick and has steel bars in each direction, which represent between 0.4 and 0.6 % of the cross-section, depending of the distance from the peripheral seals. This framework is located in the center of the upstream slope protection (Beauséjour, Bouzaïene, Hammamji, Bigras, & Bergeron, 2006).

3. Failure scenarios

3.1.Seepage

In order to describe the safety factors associated with various dam failure scenarios, we first need to describe the characteristics of seepage through dams. The height of water above the parapet (W, defined in the equation [1]) governs the water seepage through the dam. H_{res}, h_p and H_{dam} represent the height of water in the reservoir, the height of the parapet and the height of the dam (figure 1).

[1] $$W = H_{res} - H_{dam} - h_p$$

The water height on the downstream side of the crest h_e, depend on parameter W.

The overtopping wave is divided into several sections (figure 4) and h_e is calculated by an iterative process for a unit width, based on mass conservation, as follows.

1. A value of h_e is chosen to begin the process
2. The following equations (Eqs. 2 through 6) are solved with this value of h_e to yield a corresponding value of W
3. The value of h_c is systematically changed until convergence to the appropriate value of W. If the process diverges (very small value of h_c leading to a very high value of W), the seepage length l_0 (defined as the width of the crest were the seepage occurs) is smaller than the width L_c of the crest. h_c being equal to h_0, the iteration is then made on h_1 and h_c is equal to zero.

In each iteration, equations [2] to [5], the spillway formula and the Torricelli formula (Bennis, 2007) are solved.

[2] $$q_0 = m\sqrt{2gh_e^{\,3}}$$

[3] $$q'_i = C_d\sqrt{2gh_i S_{sp}^{\,2}}$$

[4] $$q_{i+1} = q_i + q'_i$$

[5] $$h_{i+1} = \left(\frac{q_{i+1}}{m\sqrt{2g}}\right)^{2/3}$$

[6] $$h_n = W$$

Where

n : Number of sections which divide the overtopping wave

q_i : horizontal discharge upstream of the i section ($m^3/s/m$)

m : spillway coefficient (-)

g : gravitational acceleration ($m.s^{-2}$)

h_i : water level in the i section i (m)

q'_i : vertical discharge in the i section ($m^3/s/m$)

C_d : seepage coefficient taking into account turbulence and the horizontal velocity (-)

S_{sp} : seepage area for a unit width, depending on the porosity (m^2/m)

q_{i+1} : horizontal discharge upstream of the i+1 section ($m^3/s/m$)

h_{i+1} : water level in the i+1 section i (m)

3.2.Landslide

The pressure of the water on the upstream concrete slope protection could result in the landslide of part of the dam. The "Multiple Wedge Analysis" method (U.S. Army Corps of Engineers, 1995) (figure 5), allows calculation of the landslide safety factors associated with different overtopping heights. After having defined the

fracture line, the safety factor is calculated based on the equilibrium of the shear strength and the applied stresses. These stresses are calculated by dividing the dam into several blocks and by calculating the forces on each of these blocks per unit width. The equation [5] gives the safety factor.

[7] $$FS1 = \frac{[(W_i + V_i)\cos\alpha_i + (H_{Li} - H_{Ri})\sin\alpha_i + (P_{i-1} - P_i)\sin\alpha_i - U_i]\tan\phi_i + C_i L_i}{(H_{Li} - H_{Ri})\cos\alpha_i + (P_{i-1} - P_i)\cos\alpha_i - (W_i + V_i)\sin\alpha_i}$$

Where

i : number defining the block (-)

$(P_{i-1} - P_i)$: sum of the horizontal forces applied on the block i ($N.m^{-1}$)

W_i : total weight, combining the effects of water, rocks and concrete ($N.m^{-1}$)

V_i : vertical force applied on the top of the block ($N\ m^{-1}$)

α_i : angle between the fracture line of the i block and the horizontal (°)

Φ_i : internal angle of friction of the i block materials (°)

U_i : upward flow force applied on the bottom of the i block ($N\ m^{-1}$)

H_{Li} : horizontal force applied on the left of the i block ($N\ m^{-1}$)

H_{Ri} : horizontal force applied on the right of the i block ($N\ m^{-1}$)

L_i : length of the fracture line of the i block (m)

C_i : cohesion of the materials of the i block (Pa)

FS1 : landslide safety factor (-)

The equations [8] and [9], once solved, give the landslide safety factor for the dam.

[8] $$\sum_i (P_{i-1} - P_i) = 0$$

Where

[9]

$$(P_{i-1} - P_i) = \frac{[(W_i + V_i)\cos\alpha_i - U_i + (H_{Li} - H_{Ri})\sin\alpha_i]\frac{\tan\varphi_i}{FS1_i} - (H_{Li} - H_{Ri})\cos\alpha_i + (W_i + V_i)\sin\alpha_i + \frac{c_i}{FS1_i}L_i}{(\cos\alpha_i - \sin\alpha_i \frac{\tan\varphi_i}{FS1_i})}$$

3.3.Motion of the crest materials

In this study of the failure scenarios, we consider that some of the overtopping water infiltrates into the dam from the crest. However, the overtopping flow rate can be high enough that this flow does not entirely infiltrate into the dam. In this case, the overtopping can lead to the motion of the rock on the downstream side of the crest. The horizontal velocity of the flow is responsible for a horizontal drag force on the rocks, balanced by the friction forces from the materials below, depending on the weight of the rock and the buoyancy force. Our goal here is to compare the drag force and the friction force by calculating a safety factor, equal to the friction force/drag force ratio, to determine if the friction force is important enough to prevent the rock from moving.

From the study of the seepage through the crest, we know the level of water on the downstream side of the crest for each value of *W*. Then, the forces acting on the rock are calculated (figure 6) : the weight *P*, the buoyancy *A*, the vertical reaction of the dam R, the drag force *D* (Etienne Guyon & Hulin, 2001), and the friction force *T* (Lancellota, 2009). Finally, the safety factor can be determined with Eq. 15.

[10] $$P = \gamma_{roc} V_r$$

[11] $$A = \gamma_{wat} V_r$$

[12] $$R = P - A$$

[13] $$D = C_D \rho V^2 \frac{A_e}{2}$$

[14] $$T = (P - A)\tan\phi$$

[15] $$FS2 = \frac{T}{D}$$

Where

γ_{roc} : unit weight of the rock (N.m^{-3})

γ_{wat} : unit weight of the water (N.m^{-3})

P : stone weight (N)

A : buoyancy (N)

R : vertical reaction of the dam (N)

V: overflow velocity ($m.s^{-1}$)

D : drag force (N)

V_r: rock volume (m^3)

A_e : vertical surface of the rock (m^2)

T : friction force (N)

Φ : internal angle of friction (°)

$FS2$: safety factor (-)

3.4.Motion on the downstream face bottom

Wilkins (1956) investigations, led to the discovery of a limit gradient equal to 1. That is, rocks are put in motion when the hydraulic gradient is greater than the limit gradient (this theory can also be found in (Lafleur, 1991)). Using the geotechnical properties of the rock fill, our goal is to estimate the water velocity in the area where the water leaves the dam, which is not only where the velocity is the greatest, but also where the rocks are more likely to start moving by the action of water. Wilkins (1956) proposed a method for estimating the depth flow exiting the downstream face of the dam, based on assuming critical flow depth corresponding to a Froude Number of 1. Equation [16] gives this depth of flow or water level.

[16] $$h_s = (q^2/g * (\frac{1+e}{e})^2)^{1/3}$$

Where

q : seepage discharge in the dam per unit width ($m^3/s/m$)

e : rock fill void ratio (-)

h_s : water level where the water leaves the dam (m)

An empirical formula which links the water velocity in the voids V ($m.s^{-1}$) and the hydraulic gradient i (-) for turbulent flows (flow through rockfill dams being high Reynolds number flows) is then used. Several formula exist in the literature ((Ergun, 1952), (Martins, 1990), (Mc Corquodale, Hannoura, & Nasser, 1978), (Stephenson,

1979), (Wilkins, 1956)). In all of these equations, g is the gravity acceleration ($m.s^{-2}$), d is the rocks diameter (m), v the cinematic viscosity ($m^2.s^{-1}$), e the void ratio (-) and n the porosity (-).

- Ergun (1952)

[17] $$i = \left(\frac{1-n}{n^3}\right)\left(\frac{150\nu(1-n)V}{gd^2} + \frac{1.75V^2}{gd}\right)$$

- Martins (1990)

[18] $$i = \frac{C_u^{\,2\alpha}}{2n^2 K_M{}^2 g.e.d} V^2$$

C_u is a uniformity coefficient ($C_u = d_{60}/d_{10}$) and α an empirical coefficient (α = 0,26). K_M is the empirical coefficient of Martins, equal to 0,56 for angular materials

- Wilkins (1956)

[19] $$i = \frac{1}{m^{0.93}}\left(\frac{V}{Wn}\right)^{1.85}$$

W is an empirical coefficient equal to 5,243 ($m^{0.495}.s^{-1}$) in the international system of units and m is the hydraulic radius (m).

- McCorquodale et al (1978)

[20] $$i = \frac{70\nu V}{gnm^2} + \frac{0.54\Psi V^2}{gn^{0.5}m}$$

[21] $$\Psi = \frac{1}{2}\left(1 + \frac{f_e}{f_o}\right)$$

f_e and f_o are friction factors of Darcy-Weisbach. f_e is the friction factor of the rocks and the permeameter, without considering the wall-effect which could have an impact on the value of the hydraulic radius (Devendra mehta & Hawley, 2002), f_o is the friction factor of an hydraulically smooth surface for the same Reynolds number. According to McCorquodale, for coarse rockfill, the f_e/f_o ratio is about 1,5.

- Stephenson (1979)

213 [22] $$i = \frac{K}{gdn^2} V^2$$

214 K_s is an empirical coefficient of Stephenson whose value is about 1,4.

215 • Ergun-Reichelt (1990)

216 [23] $$i = \left(\frac{1-n}{n^3}\right)\left(\frac{214M^2\nu(1-n)V}{gd^2} + \frac{1.57MV^2}{gd}\right)$$

217 [24] $$M = 1 + \frac{2d}{3D(1-n)}$$

218 D is the diameter of the permeameter.

219

220 Experiments have been conducted at the University of Ottawa(Hansen, Garga, & Townsend, 1995). 1D hydraulic
221 tests have been performed in a packed-column apparatus on various type of rocks and experimental results were
222 compared to the results obtained by applying the previous equations (figure 7). The Stephenson (1979) and
223 Wilkins (1956) performed the best and for high gradient and bulk velocity, the Wilkins equation appeared to be
224 the more accurate. Consequently this formula has been chosen for our investigations.
225 The velocity in the voids V_v (m/s) is given by Equation 25 as a function of discharge per unit with q ($m^3/s/m$), the
226 flow depth exiting the dam face h_s (m) and porosity n.

227 [25] $$v_v = \frac{q}{nh_s}$$

228 The safety factor *FS3* is defined as the limit gradient/actual gradient ratio:

229 [26] $$FS3 = \frac{1}{i}$$

230 Once the safety factor reaches the value of 1, the most-downstream rock is put in motion and leaves the dam;
231 consequently, another rock on the downstream face takes its place without any change of the hydraulic gradient.
232 This continues until the complete disappearance of the upper layer of the downstream face of the dam. At the end

of this process, the crest width has decreased. Consequently, the downstream layer of the dam is considered to be lost once the safety factor reaches the value of 1.

3.4.Parapet and concrete slope protection failure

In case of overtopping, the concrete mask and the parapet on the upstream side of the crest are subjected to external loads, caused by the active water pressure and the passive embankment pressure, which can lead to the failure of the structural elements of the dam. The weight of these elements is also responsible for internal loads. These loads are rectangular and triangular and depend on parameters H_{dam} (dam height) (m), L_m (mask length), h_p (parapet height) (m), W(overflow height) (m), t_m (concrete mask thickness) (m), K_p (passive earth pressure coefficient) (-), β (downstream face of the dam angle with the horizontal plane) (°) and the water, concrete and rocks weights ($N.m^{-3}$) (figures 7 and 8).

The calculation of shear forces T (N) and bending moments M (N.m) in the upstream slope protection and the parapet is followed by the calculation of shear stresses τ and bending stresses in the structural elements. In theory, the 3 dimensions of stress should be taken into account, but one dimension can be excluded. Forces are symmetrical in the axial direction of the dam, consequently the system is a plane stress situation.

The x-axis is parallel to the downstream slope protection and to the parapet and most of the stress is parallel to this axis. The y-axis is perpendicular to the x-axis and the stress in this direction is very low and considered to be equal to zero in this calculation. In addition, shear stress τ_{xy} is equal to τ_{yx}.

The shear stress is calculated in the center of the cross-section and the bending stress is calculated in the downstream and upstream ends of the cross-section (figures 10 and 11). Once the distribution of stresses is known in the structural elements, safety factors can be calculated. Both of the safety factors presented in this section are calculated in the middle and in the downstream and upstream ends of the structural elements.

Stresses per unit width are calculated with the equations [27] to [34] for the upstream slope protection. The equations for the parapet are not shown explicitly herein but can be defined with the same methodology as that used to define the stresses for the upstream slope protection (equations [27] to [34] , equations [35] and [36]).)

Where

[27] $\sigma_{x-upstream} = \sigma_{active-water-pressure} + \sigma_{passive-soil-pressure} + \sigma_{mask-weight} = -\sigma_{x-downstream}$ et $\sigma_{x-center} = 0$

[28] $$\sigma_{active-water-pressure} = \frac{t_m \gamma_{wat}}{2I} * ((h_p + W) * \frac{(L_m - x)^2}{2} + H_{barr} * \frac{(L_m - x)^3}{6L_m})$$

[29] $$\sigma_{passive-soil-pressure} = -\frac{t_m}{2I} * K_p * H_{dam} * \gamma_{soil} * \frac{(L_m - x)^3}{6L_m}$$

[30] $$\sigma_{mask-weight} = \cos\beta * \gamma_{concrete} * (L_m - x)$$

[31] $\tau_{xy-masl-middle} = \tau_{active-water-pressure} + \tau_{passive-soil-pressure} + \tau_{mask-weight}$ et $\tau_{xy-ends} = 0$

[32] $$\tau_{active-water-pressure} = -\frac{3\gamma_{wat}}{2t_m} * ((h_p + W) * (L_m - x) + H_{dam} * \frac{(L_m - x)^2}{2L_m})$$

[33] $$\tau_{active-water-pressure} = \frac{3}{2t_m} * K_p * H_{dam} * \gamma_{soil} * \frac{(L_m - x)^2}{2L_m}$$

[34] $$\tau_{mask-weight} = -\frac{3}{2} * \sin(\beta) * \gamma_{concrete} * (L_m - x)$$

And in the parapet :

[35]

$\sigma_{x-parapet-upstream} = \sigma_{active-water-pressure} + \sigma_{passive-water-pressure} + \sigma_{parapet-weight} = -\sigma_{x-parapet-downstream}$ et $\tau_{xy-parapet-ends} = 0$

[36] $\sigma_{x-parapet-middle} = 0$ $\tau_{xy} = \tau_{xy-parapet-middle}$

From the triplet (σ_x ; σ_y ; τ_{xy}), the principal stresses σ_1 and σ_3 are calculated (by convention $\sigma_1 > \sigma_3$) using the properties of the Mohr's circle (figure 11) (André Bazergui, Bui-Quoc Thang, & André Biron, 2002).

[37] $$\sigma_1 = \frac{\sigma_x + \sigma_y}{2} + \sqrt{(\frac{\sigma_x + \sigma_y}{2})^2 + \tau_{xy}{}^2}$$

[38] $$\sigma_3 = \frac{\sigma_x + \sigma_y}{2} - \sqrt{(\frac{\sigma_x - \sigma_y}{2})^2 + \tau_{xy}{}^2}$$

Then the safety factor defined by (Masson, 2009) is used :

277 [39] $$FS4 = \frac{\tau_{ff1}}{\tau_f}$$

278 τ_f is the stress tangential to the fracture surface (kN/m^2) and τ_{ff1} is the stress tangential to the fracture surface when
279 the fracture occurs (kN/m^2). The knowledge of the Mohr's circle radius R and the distance P between the center of
280 the circle and the origin enable calculation of these two parameters.
281 Stresses (σ_f ; τ_f) are obtained by drawing a line perpendicular to the Coulomb line which cuts the center of the
282 Mohr's circle. Then, the fracture shear stress τ_{ff1} is calculated with a normal stress of σ_f (figure 10).
283 With $\Phi_{concrete}$ and $c_{concrete}$ being the internal angle of friction and the cohesion of concrete:

284 [40] $$\tau_f = R\cos\Phi_{concrete}$$

285 [41] $$\sigma_f = P - R\sin\Phi_{concrete}$$

286 [42] $$\tau_{ff1} = \sigma_f * \tan\Phi_{concrete} + c_{concrete}$$

287 Masson (2009) also proposes a second safety factor FS4' defined as the R_{f2}/R ratio
288 With :
289 R_{f2} : distance between the center of the Mohr's circle and the Coulomb line

290 [43] $$FS4' = \frac{R_{f2}}{R} = \frac{c_{concrete} * \cos\Phi_{concrete} + P * \sin\Phi_{concrete}}{\frac{|\sigma_1 - \sigma_3|}{2}}$$

291 **3.5.Hydrographs determination**

292 The calculation of the safety factors defined in the previous sections in each step of the dam failure allows
293 determination of the failure scenario and the corresponding hydrograph for different conditions of overtopping.
294 The corresponding hydrograph is then compared to the hydrograph obtained by using the standard procedure.
295

296 **3.5.1. Standard procedure's hydrograph**

297 The standard procedure specifies 30 minutes long failure scenario with a breach of trapezoidal cross section
298 having 45 degrees banks and a bottom width of four times the maximal height of the dam. The standard

299 procedure's hydrograph is obtained by calculating the breach discharge at each time step of 30 s, considering a
300 linear volume/elevation law and the evacuation law of a broad-crested trapezoidal weir (Marche, 2008):
301
302 [44] $$Q_b = c_v k_s \left[1,7 b_1 \left(h - h_b \right)^{1.5} + 1,26 z \left(h - h_b \right)^{2.5} \right]$$
303 Where
304 c_v : correction coefficient of the approach velocity ($m^{0.5}.s^{-1}$)
305 k_s : correction coefficient of the overtopping (-)
306 b_1 : instantaneous width of the bottom of the breach (m)
307 h_t : instantaneous water level downstream (m)
308 h : water level upstream (m)
309 h_b : bottom of the breach level (m) :
310 z : breach walls slope (-)
311 [45] $$\begin{cases} k_s = 1 - 27.8\left(\frac{h_t - h_b}{h - h_b}\right)^3 & \text{if} \quad \frac{h_t - h_b}{h - h_b} > 0.67 \\ k_s = 1 \ \text{ if not} \end{cases}$$
312
313 ### 3.5.2. Hydrograph from the safety factors methodology
314 The iterative procedure described in the figure 13 allows the identification of the failure scenario via the
315 calculations of the different safety factors and by taking into account changes of the dam geometry (H_{soil} is the
316 height of the materials behind the mask and H_{mask} the height of the mask, these parameters are used in the
317 calculation of the safety factors) . The methodology of the procedure is based on the following principles:
318 - The initial dam geometry and hydraulic conditions are defined for the first iteration
319 - At each iteration, the safety factors are calculated
320 1. FS1 : if FS1 is less than 1, the dam fails and the procedure ends.

2. FS2 and FS3 : less than 1 values of this safety factors lead to a new geometry of the dam and potential loss of the fractured part of the upstream slope protection if the crest is lower than the top of the mask
3. FS4 : if FS4 is less than 1, a fracture occurs in the mask

4. Application of the methodology

The flood scenario used to demonstrate our methodology is a gradual increase of the water level in the reservoir. The flood discharge is the MPF discharge (5630 m^3/s) and this discharge remains constant during the failure (the hypothesis of a changing discharge would not modify the methodology but would add a calculation step in order to take into account the variations in discharge). In our example scenario, we consider the spillway capacity to be reduced from 2400 m^3/s to 1000 m^3/s. With a flood discharge of 5630 m^3/s and a spillway discharge of 1000 m^3/s, the reservoir is filled with a discharge of Q_r = 4630 m^3/s.

In the case of a gradual increase of the water level in the reservoir, at t=0 the water level reaches the maximum level of operation, H_{op} = 74.9 meters. When the overtopping reaches 1.7 m over the crest (about 40 h after the beginning of the flood), the downstream slope protection fails, from the crest to the bottom. Nevertheless, the mask and the parapet stay static. The seepage discharges are assumed to be negligible compared to the flood discharge and consequently the water level still rises. The next critical overtopping level, 2.15 m, which occurs 6h20 after the slope protection has failed (which is the time needed for the water level to reach a 2.15 m overtopping in this conditions of discharge for a linear volume/elevation relation of the reservoir), leads to the failure of the parapet.

The failure of the parapet on the whole length of the dam instantly releases a 2.50 m high overtopping flow corresponding to a discharge Q_l of 3180 m^3/s. The filling of the reservoir continues with a discharge of Q_r-Q_l = 1450 m^3/s. The effect of this discharge is considered to have no impact on the water level during the failures of the downstream face and the crest which are quick mechanisms (similar to landslides). When the first fragment of the upstream concrete slope protection is gone, this releases a 6.75 m high overtopping. The safety factor linked to

346 the motion of the crest materials decreases, less than 1 (0.65). The dam failure goes faster as the failure
347 mechanisms build up.
348 The failure hydrograph starts when the parapet breaks, about 46 h after the beginning of the rising of the water
349 level in the reservoir. The discharge at t=0 starts at 3180 m^3/s. It suddenly reaches 17 700 m^3/s when the first
350 piece of the mask is taken away. It keeps increasing per stage each time another piece of the mask disappears.
351 Considering that the failure mechanisms involved are fast (as landslides), the hypothesis of a 10 min long failure
352 is taken here, with a linear increase of the discharge until the dam has totally disappeared. The drawdown is then
353 calculated with the spillway formula.

354 The corresponding failure hydrograph is compared to the standard procedure hydrograph.
355

356 5. Discussion

357 5.1.Comparaison with the standard procedure

358 This section compares the standard procedure of dam breach used in Quebec, Canada, to our methodology
359 described in this paper, by describing the physical mechanisms involved in the dam failure. In the case of dam
360 overtopping, the standard procedure assumes a failure by erosion which starts with the dam overtopping. The
361 breach develops in 30 min and its final bottom width reaches 4 times the maximal dam height. For earth dams
362 during overtopping, this well describes the failure scenario. The failure indeed begins in the low point of the crest
363 almost as soon as the overtopping occurs (depending on the materials) and the flow energy is then responsible for
364 the formation and development of the breach.
365 The methodology described in this article leads to a different conclusion for a rockfill dam with an upstream
366 concrete slope protection. A minimal overtopping level of several meters is necessary for the failure to occur,
367 because of the concrete protection. In addition, the failure no longer begins in the low point, but can concern the
368 whole width of the dam, which leads to a maximum discharge higher than calculated with the standard's
369 hypothesis. Moreover, this maximum discharge is also reached faster because the mechanisms involved are faster
370 than erosion mechanisms.

5.2.Comparison with literature results

When the whole theoretical process of failure can't be described yet, laboratory tests results gave several conclusions regarding the final geometry of the breach and the failure duration (Franca and Almeida, 2002). These experimental studies used a Froud Number similarity to take into account the scale effect. Some of the results defend the hypothesis and conclusions of the present paper and some others qualify them. Concerning the initial width breach, the experiments conclude on a large initial breach, contrary to the earthfill initial breaches, of about 1 times the dam height. In our methodology, the assumption of a large initial breach has also been made, but on the whole width of the dam, as a pessimist hypothesis.

The total failure time observed in the models was about 450 and 1200 s, which correspond to time between 1 and 2 hour and a half for a 25 m high dam. This total failure time of the dam is one of the most important parameters in the model and also the most difficult to adjust. While experimental models (Franca and Almeida, 2002) conclude on a total time failure of more than an hour, some historical data from rockfill dam failure due to overtopping only give total time failure of less than 30 min (Goose Greek dam, (Sing ans Scarlatos, 1988)). For the hypothesis of the model presented in this paper, the total time failure has been taken equal to 10 minutes. This choice has been based on the minimum time observed in historical data (less than 30 minutes) and by considering the parapet in the Toulnustouc dam. This parapet induces indeed an initial level of water much higher than in a parapet-free dam and consequently the hydraulic conditions are worse.

5.3. Limitations of the methodology

It is obvious from the historical data, experimental results and theoretical calculation that the failure of rockfill dams isn't well understood. Actual models usually don't take into account all the details of rockfill dam breaches and previous studies estimate the uncertainty of about 50% in the estimate of the maximum discharge with the actual models (CADAM, 2000). The model of our methodology allows considering more details and phenomenon of the dam breach but some aspects could be improved.

Further verifications could be necessary in order to confirm the validity of some formulas. These formulas are used here in conditions which can be different from the conditions for which they have been validated. For example the Wilkins formula is a 1D formula and is used here in a 2D application.

Hypothesis about the breach width and total time failure had to be made and are based partially on experimental and historical data. Improvements such as investigations on the initial width of the breach linked to the initial water level, rock sizes or the downstream dam slope would complete the analysis of the dam failure.

Finally, sensitivity analysis of the safety factors in our methodology was conducted with the following conclusions: When changing the values of the parameters (such as the drag force coefficient, the prorosity etc.), the calculation of the critical overflow level leading to the failure of the dam gives different results, but the orders of magnitude remains the same, as for the overall failure scenarios. Consequently, the unavoidable approximations of some parameters doesn't question the validity of the results.

6. Conclusion

The methodologies we present in this article permit the consideration of several failure mechanisms, but these mechanisms can also be linked to obtain a failure scenario which takes into account all of them. It also leads to the determination of a failure hydrograph, depending on the scenario for the rising water level.

In addition, it highlights the role of the impermeable upstream concrete slope protection which allows using an embankment with large voids (associated with large rock sizes) and is resistant to the effects of overtopping, wind and rain. The effect of the upstream concrete slope protection is that it inhibits the seepage rate through the dam. On another hand, the framework minimizes the size of the splits in the slope protection and the importance of the seepage.

This study tends to question the applicability of the standard procedures for assessing dam failures to rockfill dams with upstream concrete slope protection. Due to the erosional resistance characteristics of the materials, the overtopping scenario does not necessarily lead to the failure of the dam, but can also lead to more hazardous

scenario and more important consequences than predicted by the standard procedure, as much higher peak flow rate and shorter time-to- The results are validated by the solidity of the formula and concepts used to develop it, the consistency of the results and the physical analysis of the earth and rockfill dam's failures.

The methodology could be extended to other rockfill dams with upstream concrete slope protection and crest structures such as parapets, to confirm the conclusions of the article and add precisions on the total failure time and initial failure width parameters. Laboratory experiments could also be realized in order to include the influence of pre-failure overtopping duration in this methodology. The confirmation of the conclusions of this article would highlight the need to reconsider safety measures in case of overtopping of embankment dam with an upstream concrete slope protection.

Références

André Bazergui, Bui-Quoc Thang, & André Biron. (2002). *Résistance des matériaux (3e éd)*: Montréal : Presses internationales Polytechnique.

Beauséjour, N., Bouzaïene, H., Hammamji, Y., Bigras, A., & Bergeron, A. (2006). *Conception du barrage et de la digue sud de l'aménagement hydroélectrique de la Toulnustouc*. Paper presented at the Congrès annuel 2006 de l'ACB.

Bennis, S. (2007). *Hydraulique et hydrologie*. Presses de l'Université du Québec. 2ème édition, 476 pp.

CADAM : Concerted Action on Dambreach Modelling (2000), Final report, January

Devenda mehta, & Hawley, M. C. (1969). Wall effect in packed columns. *Ind. Eng. Chem. Process Design and Dev*elopment, *8* (2), pp 280–282

Ergun, S. (1952). Flow of water through packed columns. *Chemical Engineering Progress, 48*(2).

Etienne Guyon, & Hulin, H.-P. (2001). *Hydrodynamique physique*: EDP Sciences.

Franca, M.J. and Almeida, A.B. (2002), Experimental Tests on Rockfill Dam breaching Process. *IAHR - International Symposium on Hydraulic and Hydrological Aspects and Safety ssessment of Hydraulic Structures, St. Petersburg, May*

Hansen, D., Garga, V. K., & Townsend, D. R. (1995). Selection and application of a one-dimensional non-Darcy flow equation for two-dimensional flow through rockfill embankments. *Canadian Geotechical Journal, 32*, 223-232.

Lafleur, J. (1991). *Introduction à la géotechnique*: Presses internationales Polytechnique.

Lancellota, R. (2009). *Geotechnical Engineering (2e éd)*: Taylor & Francis Group.

Marche, C. (2008). *Barrages, crues de rupture et protection civile*: Presses Internationales Polytechnique.

Martins, R. (1990). Turbulent seepage flow through rockfill structures. *Water Powr and Dam Construction, March, 90*, 41-45.

Masson, L. (2009). *Évaluation du gain de sécurité relié au réhaussement d'une digue munie d'un élément d'Étanchéité rigide.* École Polytechnique de Montréal, Montréal.

Mc Corquodale, J. A., Hannoura, A. A., & Nasser, M. S. (1978). Hydraulic conductivity of rockfill. *Journal of Hydraulic Research, 16*(2), 123-137.

Singh, V.P. and Scarlatos, P.D. (1988). Analysis of Gradual Earth-Dam Failure., *Journal of Hydraulic Engineering., ASCE* 114(1), 21-42.

Stephenson, D. (Ed.). (1979). *Rockfill in hydraulic engineering.* Amsterdam, Netherlands.

U.S. Army Corps of Engineers. (1995). *Gravity Dam Design* (Vol. EM 1110-2-2200). Honolulu: University Press of Pacific.

Wilkins, J. K. (1956). *Flow of water through rockfill and its application to the design of dams*. Paper presented at the New-Zealand Conference on Soil Mechanics and Foundation Engineering.

Figures list

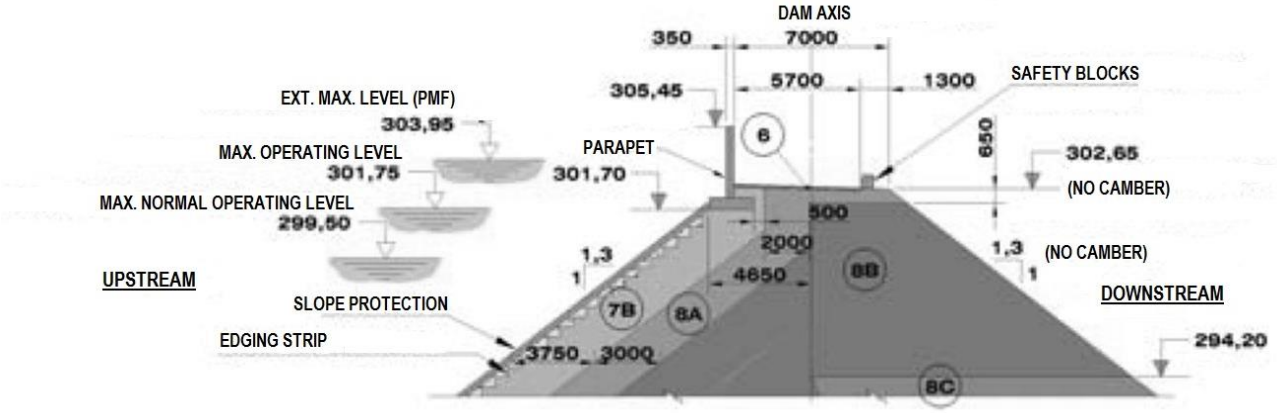

487
488 Fig.1. Cross section of the Toulustouc dam (Beauséjour, et al., 2006)

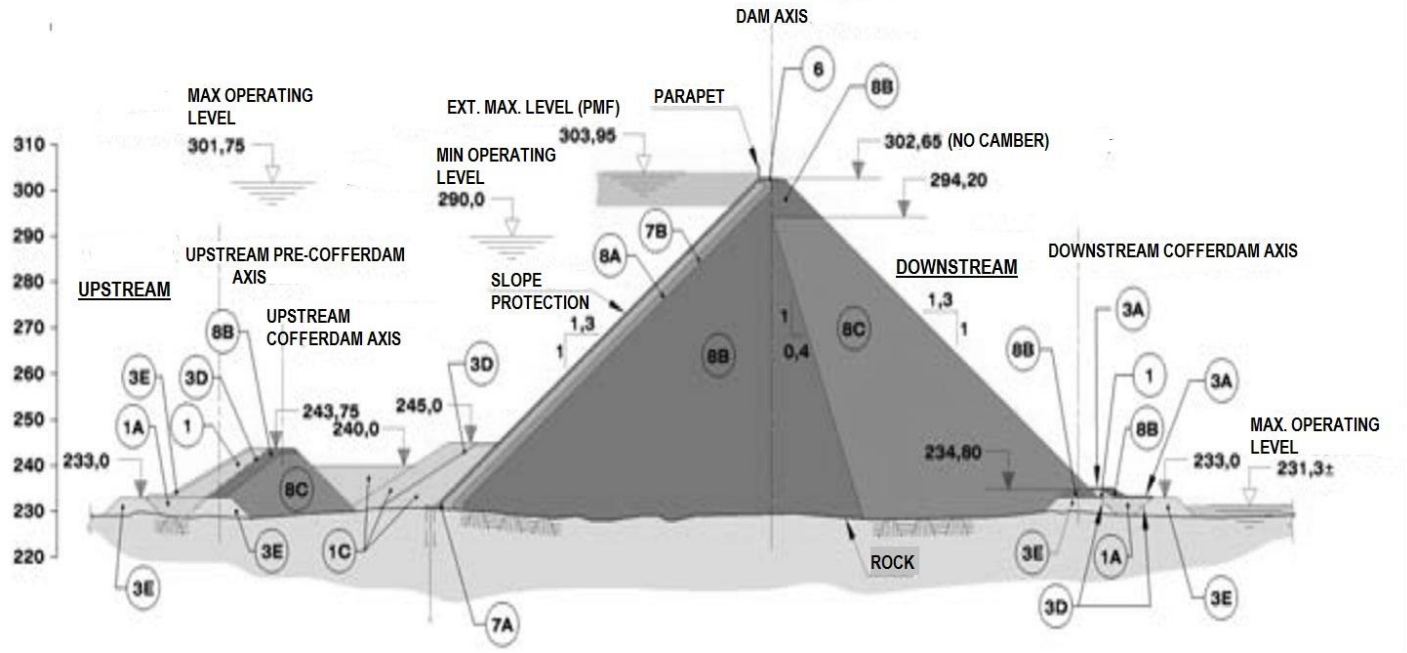

489
490 Fig.2. Cross section of the Toulnustouc dam crest (Beauséjour, et al., 2006)

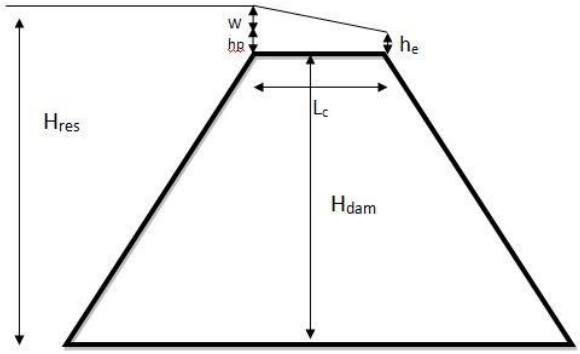

491
492 Fig.3. Crest seepage calculation

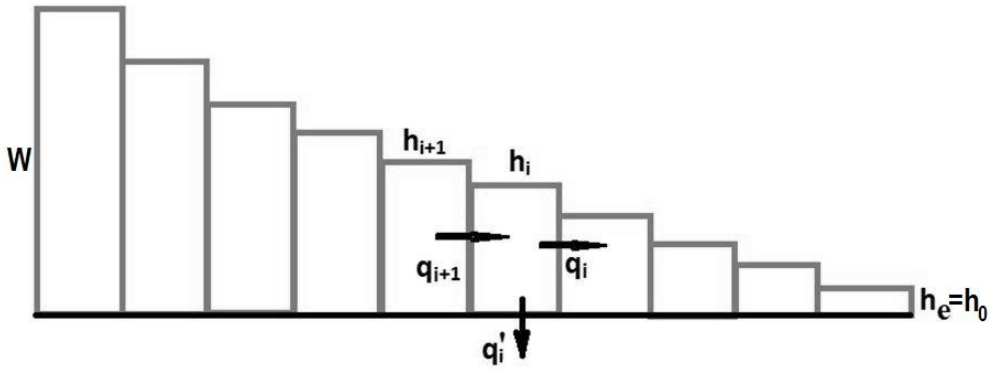

493
494 Fig.4. Illustration of the "Multiple Wedge Analysis" method (US Army Corps of Engineers, 1995)

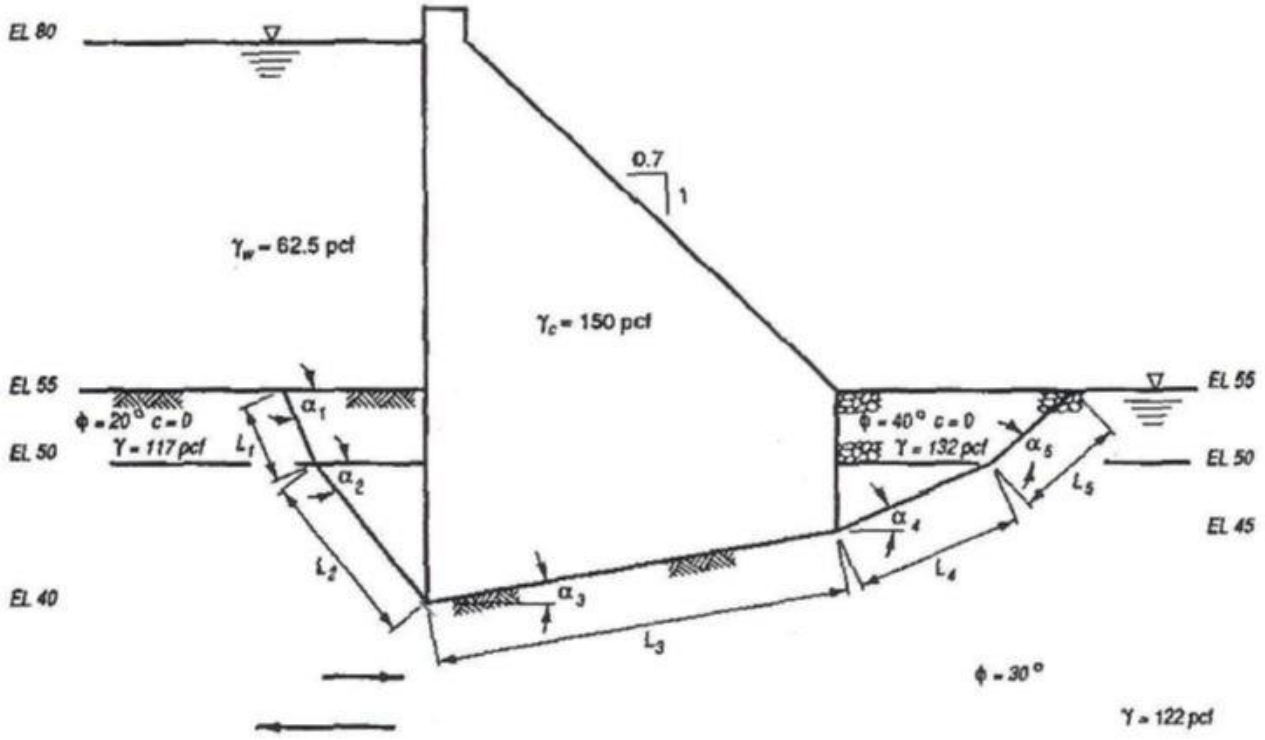

495
496 Figure 5_ Multiple Wedge Analysis (US Army Corps of Ingineers, 1995)

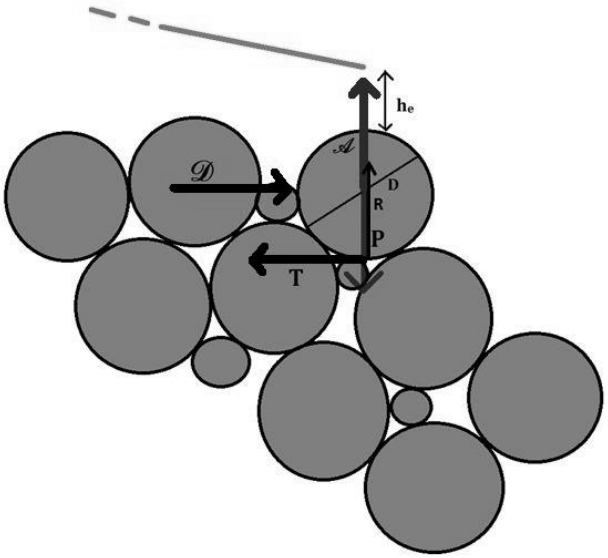

497
498 Fig.6. Forces affecting the blocks

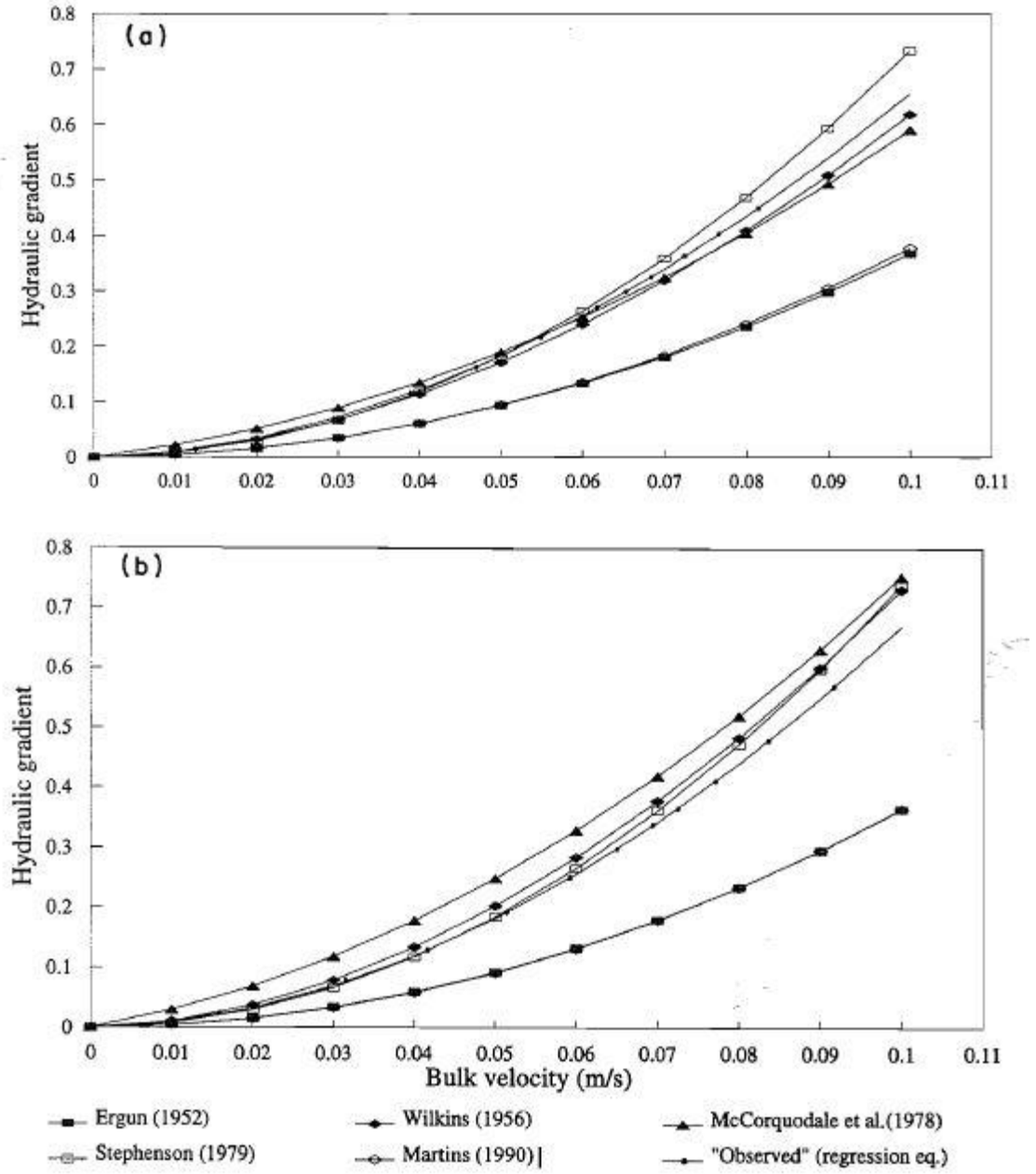

Fig 7. Flow through rockfill experiments (Ottawa)

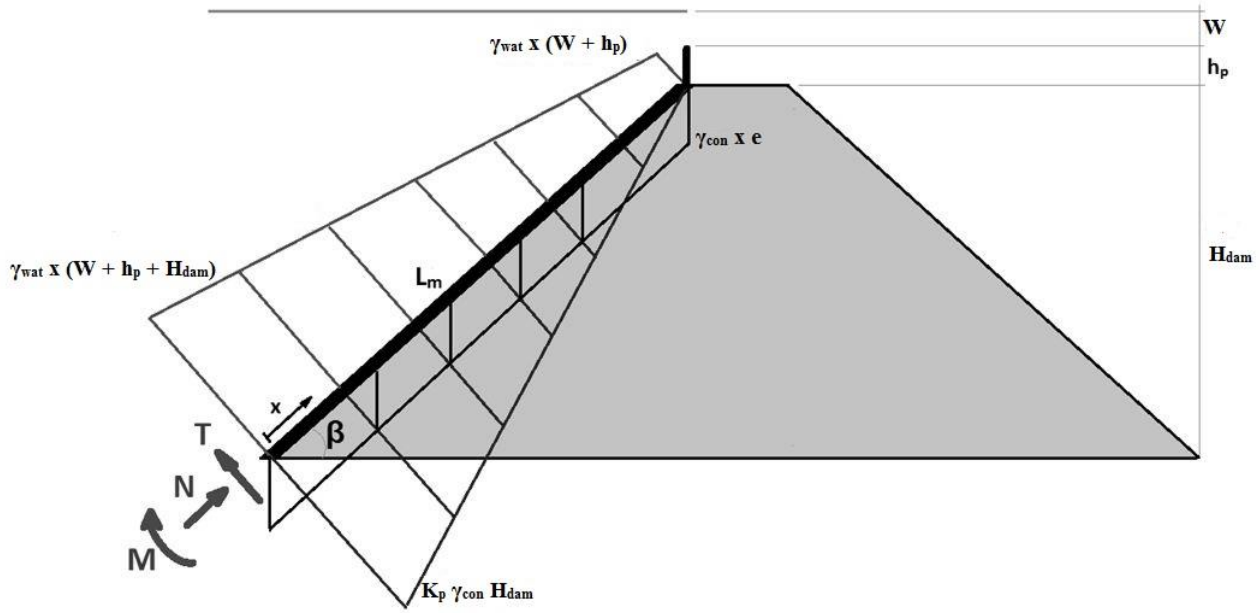

Fig.8. Stresses on the parapet

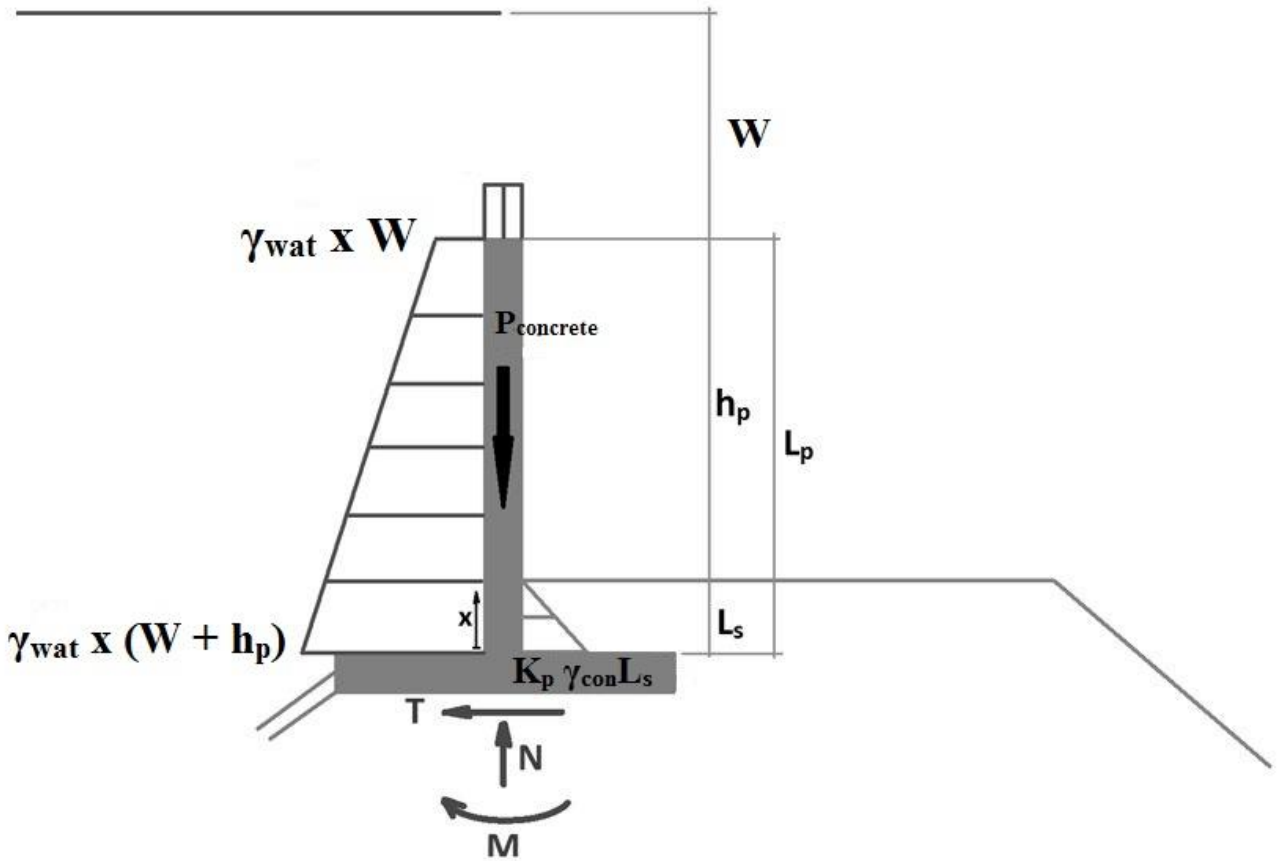

Fig.9. Stresses on the upstream mask

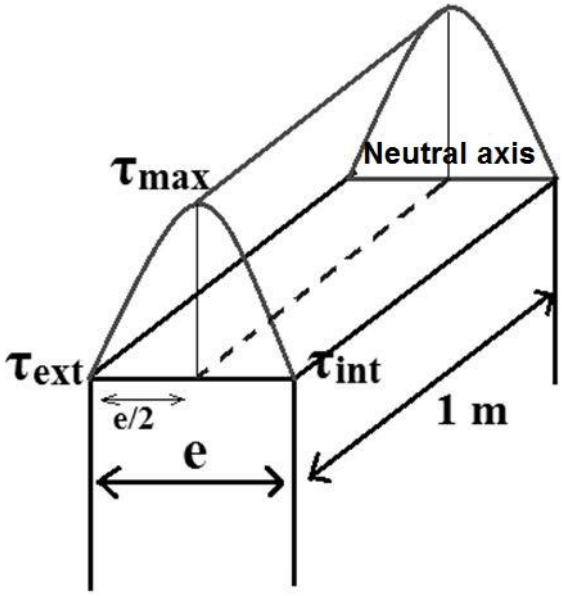

507
508 Fig.10. Distribution of normal stresses

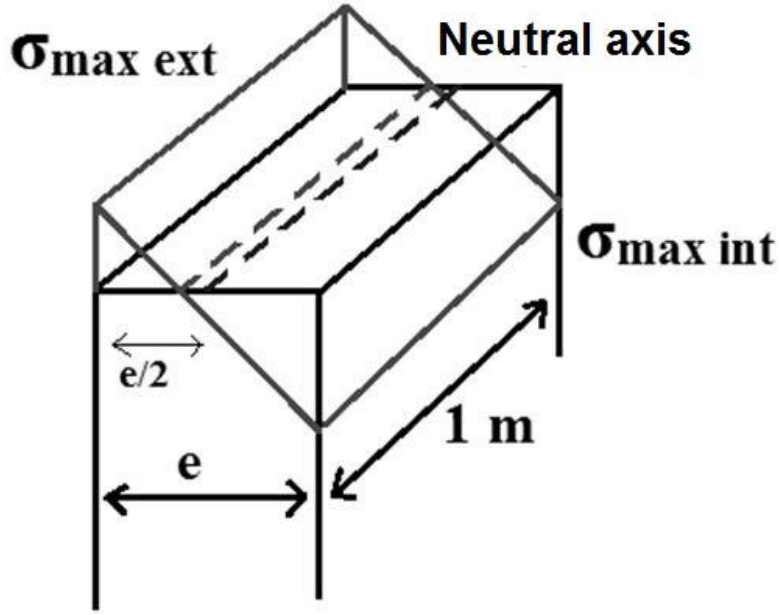

509
510 Fig.11. Distribution of shear stress

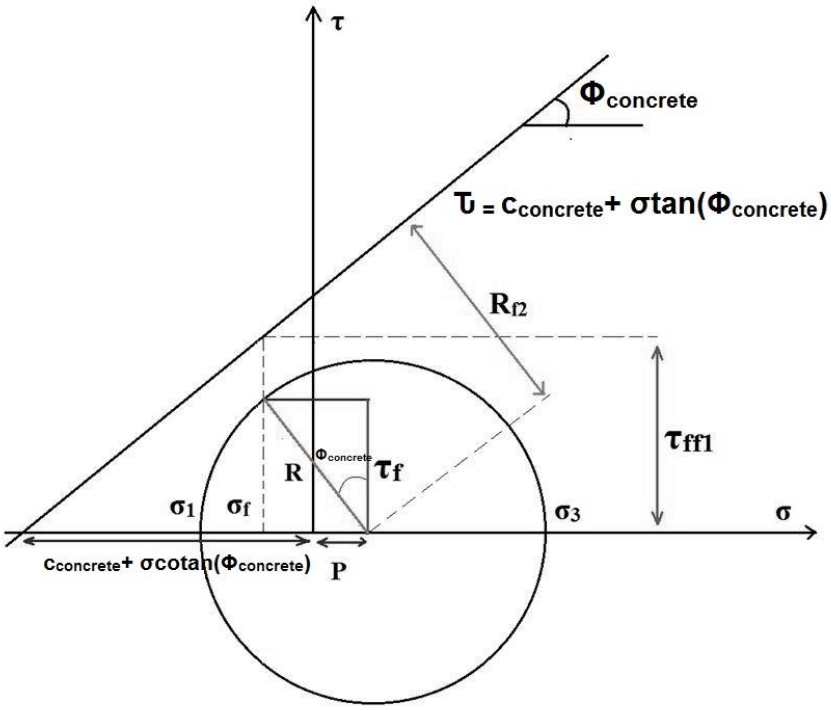

511
512 Fig.12. Mohr-Coulomb failure criteria and safety factor FS4 et FS4'

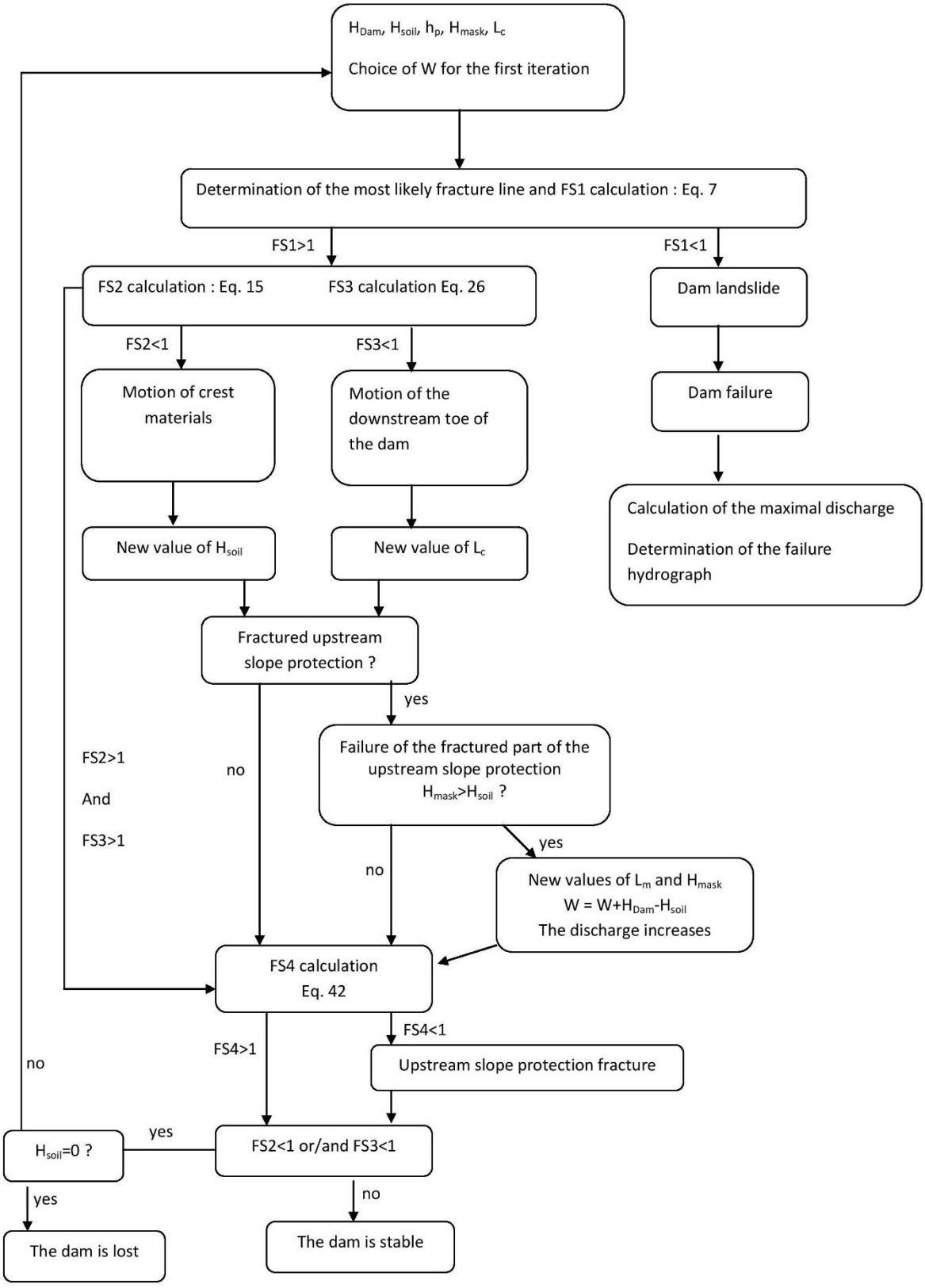

513
514 Fig.13. Failure scenario calculation process

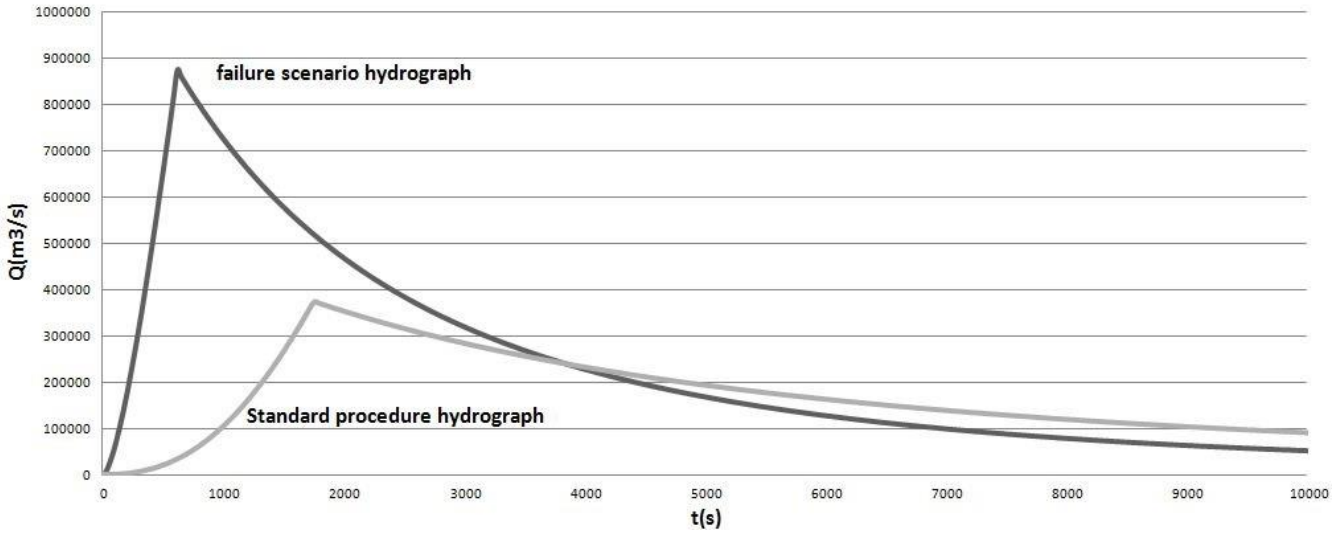

Fig.14. Comparison of the hydrographs from the norm application and from the methodology